AN LDA INVESTIGATION OF THREE-DIMENSIONAL NORMAL SHOCK WAVE BOUNDARY-LAYER INTERACTIONS

R.M. Chriss,
W.R. Hingst, and
A.J. Strazisar
NASA Lewis Research Center
Cleveland, Ohio

T.G. Keith, Jr.
University of Toledo
Toledo, Ohio

ABSTRACT

Nonintrusive measurements have been made of a normal shock wave/boundary-layer interaction. Two-dimensional measurements were made throughout the interaction region while three-dimensional measurements were made in the vicinity of the shock wave. The measurements were made in the corner of the test section of a continuous supersonic wind tunnel in which a normal shock wave had been stabilized. LDA,[*] surface pressure measurement and flow visualization techniques were employed for two freestream Mach number test cases: 1.6 and 1.3. The former contained separated flow regions and a system of shock waves. The latter was found to be far less complicated. The reported results define the flowfield structure in detail for each case.

INTRODUCTION

Normal shock wave/turbulent boundary-layer interactions occur in a number of important high-speed flow applications. These include, for example, flows within turbomachines, transonic flows over wings and external surfaces, and supersonic flows within inlet systems. The present investigation is relevant to the latter application.

It is well known that large pressure gradients associated with shock-boundary-layer interactions have the potential of producing large regions of separated flow. These, in turn, can cause a substantial degradation of inlet performance. Consequently, to design improved high-speed flow components, where normal shocks occur, a thorough understanding of the flow physics and the capability to compute the interaction is necessary. This is made more difficult by the fact that in internal flow applications with the exception of purely axisymmetric flows, normal shock-boundary-layer interactions are three-dimensional.

In this investigation a normal shock wave was stabilized in a square wind tunnel test section and was allowed to freely interact with the naturally occurring tunnel sidewall boundary layers. The emphasis was in making nonintrusive three-dimensional measurements in the corner of the test section in order to determine the flowfield associated with the interaction.

Two-dimensional measurements (of u and v) were made throughout the flowfield. The third component (w) was measured only in the corner near the the shock, where it was

[*]Laser-Doppler anemometry(LDA).

expected to be significant. The results will be presented in the form of Mach number contours in addition to secondary flow vector plots where the z component (w) was measured. The effect of the third component on the Mach number, where w was measured, is expected to be small due to the small flow angles encountered.

Two entirely different flow structures are known to exist for two-dimensional flows at freestream Mach numbers of 1.6 and 1.3. In addition, the Mach 1.3 flow is known to be near the limit for the onset of separation. It is thought that the ultimate test for any computational scheme which aims to provide accurate internal compressible flowfield predictive capability would be to model these two flow structures.

Previous work has been limited to two-dimensional interactions either along the center plane of rectangular flow geometries or to axisymmetric configurations, (refs. 1-15). Moreover, much of the existing data was obtained with pitot pressure probes. The sensitivity of the normal shock to these intrusive measurement techniques has limited the progress in the study of these flows.

Seddon (ref. 1), used static pressure probes to produce the benchmark model of the two-dimensional interaction shown in Fig. 1. Two-dimensional investigations by Abbiss, et al. (ref. 14) and East (ref. 15) have employed laser-Doppler anemometry (LDA). However, in addition to being two-dimensional, the scope of these investigations were limited to the interaction region only and did not describe the flowfield far downstream of the interaction.

In the following, the experimental apparatus employed, as well as the various measurements made during the course of the tests will be described. Estimates of the experimental uncertainty in the measured data are made. Finally, results from a flow visualization investigation, from surface pressure measurements and from LDA flowfield surveys are presented and discussed.

NOMENCLATURE

a_{ij}	elements of a 3 x 3 calibration matrix used to convert the measured LDA velocity components into orthogonal values.
a_t	speed of sound based on total temperature.
e	error.
k	ratio of specific heats.
M	Mach number.
N	number of LDA realizations per channel.
s	estimate of the standard deviation.
u,v,w	orthogonal time averaged, velocity components along the x,y and z directions.
z_c	confidence coefficient.
γ	flow angle in the x-y plane.
Δ	error or change appearing in the parentheses.
θ	angle in the x-y plane between the x axis and LDA channels 1 and 2.
ϕ	angle in the x-z plane between the x axis and channel 3.
subscripts	
u,v,w	refers to the x,y or z velocity components.
$1,2,3$	LDA channel number.

EXPERIMENTAL MEASUREMENTS AND EQUIPMENT

Facility

A normal shock wave was stabilized in the test section of the NASA Lewis Research Center's 30.5cm x 30.5cm (1 foot x 1 foot) supersonic wind tunnel, which is an open circuit, continuous-flow facility, Fig. 2. Tests were performed at nominal freestream Mach numbers of 1.6 and 1.3. The shock was established by placing a conical obstacle in the diffuser approximately 1.2 meters (4 feet) downstream of the wind tunnel test section. A schematic of the coordinate system used in the investigation is shown in Fig. 3. In both test cases, the freestream shock was maintained at x = 10cm (3.9 inches). The shock interacted with the naturally occurring tunnel wall boundary layers. The flow Reynolds number for both tests was 15 x 10^6/meter.

A preliminary schlieren investigation indicated high-frequency oscillations in the shock wave location. This was suspected from previous studies and is thought to be caused by the inherent instability of a normal shock in a constant area duct. In addition, the oscillation may be exacerbated by the turbulence of the approaching boundary layer as well as disturbances arising in the separation regions which emanate within the boundary layer throughout the interaction region. The shock position oscillated about its mean location with a magnitude of approximately ±1 cm (0.4 inches). Its mean location could be adjusted or maintained by actuation of the cone blockage as required. These oscillations manifested themselves in the form of bimodal histograms that were obtained during LDA surveys near the shock. The mean shock location was monitored by wall surface static pressure measurements (time smoothed) in order to assure that there was no movement of the shock during the lengthy flowfield surveys.

The tunnel total pressure was maintained at 103.4 and 97.9 kPa (15.0 and 14.2 psia) for the 1.6 and 1.3 cases respectively. The total temperature varied between 10 and 20°C (50 and 70°F) throughout the tests.

Flow Visualization

Qualitative measurements of the interaction were made with schlieren and surface oil flow visualization techniques. Collectively, these two qualitative techniques provide valuable insight into the flow physics.

Floor Static Pressure Measurements

Static pressure measurements were made across the floor of the test section at 72 locations. These measurements were used to demonstrate flow symmetry as well as to monitor the shock location during the tests in addition to providing important pressure recovery information.

The Laser Anemometer

Three velocity components were obtained in this investigation: u and v in the x-y plane and w along the optical axis. A single component laser anemometer was used in off-axis forward scatter. The x and y velocity components (u and v) were obtained by rotating the beams about the optical axis. The z component (w) was obtained by rotating the entire system about the y axis. The LDA system obtained data in a nonorthogonal coordinate system depicted in Fig. 4. The LDA system employed had an angle θ of 30° and an angle ϕ of approximately 28°. The anemometer was mounted on a computer controlled 4-axis table and the measurements were monitored with a real time

graphics display that included velocity histograms. This capability is considered to be important in maintaining the accuracy of the velocity measurements.

Since the flow in the tunnel was quarter symmetric as demonstrated by examination of the wall static measurements, laser anemometer measurements were acquired in only one quadrant of the test section. The measurements were performed in the upper half of the test section due to the tendency of the seed oil to deposit on the lower half of the windows much faster than on the upper half. For clarity, however, the measured values are presented in terms of the right hand coordinate system shown in Fig. 3. The flowfields were investigated in detail by surveying along both the axial and cross section planes. Each survey plane contained on the order of 1000 individual measurement locations. The complete set of data for each freestream Mach number contained approximately 20,000 measurement locations.

The data rate was normally maintained at 1000 realizations per second. At startup with clean windows, the data rate could be adjusted up to 10,000 realizations per second without affecting the accuracy of the data. During the tests, the windows of the test section gradually became fogged with seed oil. For the Mach 1.6 tests, the tunnel could normally be run from 2 to 4 hours before the windows required cleaning. For the 1.3 case, the rate of contamination was greatly reduced so that 5 to 8 hour runs were typical.

A TSI Inc. 1990B signal processor was used, together with a PDP 11/34 Digital Computer, to aquire and record the data. The data were reduced on a VAX 11/750 computer and transferred to an IBM 3033 in order to make use of a three-dimensional graphics capability.

The Particle Generator
It is well known that in high speed flows, containing large velocity gradients, lag of the seed particles is a major experimental concern. The seed particles must be sufficiently small and bouyant enough to follow the flow closely so as to maintain accurate resolution of the data. An evaporation condensation generator (refs. 16-18) was designed and built in order to produce Dioctyl Phthalate (DOP) particles with a mean diameter of 0.8 micron. From previous investigations (refs. 19-20), it was known that this size is small enough to permit the particles to track the flow with sufficient integrity but yet large enough to produce a strong LDA signal.

The seed droplet distribution was observed in situ with a TSI, Inc. Aerodynamic Particle Sizer (APS 33), Fig. 5. The on-line LDA data provided an independent check on the seeding technique, i.e., as the shock oscillated about the probe volume while surveying near the shock, the resulting velocity histograms were distinctly bimodal, Fig. 6, indicating a monodisperse seed distribution.

ERROR AND UNCERTAINTY ANALYSIS

Error Analysis
The maximum uncertainty due to omitting the z component from the velocity and Mach number calculations can be approximated by assuming that this component has the same magnitude as the y velocity component, i.e., $w \approx v$. Thus, the flow velocity is approximated by $\sqrt{u^2 + 2v^2}$. If the w velocity component is completely ignored, the velocity would then be $\sqrt{u^2 + v^2}$. The resulting error by making this omission can be

approximately written as

$$e = 1 - \left\{ \frac{u^2 + v^2}{u^2 + 2v^2} \right\}^{1/2} = 1 - \left\{ \frac{1 + \tan^2\gamma}{1 + 2\tan^2\gamma} \right\}^{1/2} \tag{1}$$

where γ is the flow angle in the x-y plane. Outside the region where the z component (w) was measured the largest flow angle γ encountered was approximately $10°$ and $5°$ for the 1.6 and 1.3 cases respectively. With these flow angles the largest error in omitting w in the total velocity would be approximately 1.5% and 0.4% respectively.

The Mach number throughout the flowfield can be computed from

$$M^2 = (V/a_t)^2 \left\{ 1 - \frac{k-1}{2} (V/a_t)^2 \right\}^{-1} \tag{2}$$

where a_t is the speed of sound calculated at the total temperature, $V = \sqrt{u^2 + v^2 + w^2}$, and k is the ratio of specific heats. This equation is valid for thermally and calorically perfect gases undergoing adiabatic processes. Using this expression and the velocity approximations described above, the maximum error expected in the Mach number due to omitting w would be approximately 3% and 1% for the respective 1.6 and 1.3 freestream Mach number cases.

Statistical Considerations

For the coordinate system shown in Figs. 3 and 4, it can be seen that the velocity components u,v and w can be written in terms of v_1, v_2 and v_3 (the velocity components as measured by LDA channels 1,2, and 3 respectively) as follows

$$
\begin{aligned}
u &= \frac{v_1 + v_2}{2\cos\theta} \\
v &= \frac{v_1 - v_2}{2\sin\theta} \\
w &= -\frac{u}{\tan\phi} + \frac{v_3}{\sin\phi}
\end{aligned} \tag{3}
$$

where θ is the angle in the x-y plane between the x axis and channel 3. Snyder, et al. (ref. 21) have pointed out that this set of equations, for a generalized three-dimensional LDA system, can be expressed in matrix form as

$$
\left\{ \begin{array}{c} u \\ v \\ w \end{array} \right\} = \left\{ \begin{array}{ccc} a_{11} & a_{12} & a_{13} \\ a_{21} & a_{22} & a_{23} \\ a_{31} & a_{32} & a_{33} \end{array} \right\} \left\{ \begin{array}{c} v_1 \\ v_2 \\ v_3 \end{array} \right\} \tag{4}
$$

Thus, $a_{11} = a_{12} = (1/2)\cos\theta, a_{13} = 0$, etc.

For uncorrelated data, i.e., measurements made from different seed particles by a non-simultaneous LDA system, it has been suggested (ref. 21) that the variances associated with each of the coordinate directions x,y and z can be expressed in terms of the variances s_1^2, s_2^2 and s_3^2 of the velocity ensembles of the three LDA channels in the following manner

$$
\left\{ \begin{array}{c} s_u^2 \\ s_v^2 \\ s_w^2 \end{array} \right\} = \left\{ \begin{array}{ccc} a_{11}^2 & a_{12}^2 & a_{13}^2 \\ a_{21}^2 & a_{22}^2 & a_{23}^2 \\ a_{31}^2 & a_{32}^2 & a_{33}^2 \end{array} \right\} \left\{ \begin{array}{c} s_1^2 \\ s_2^2 \\ s_3^2 \end{array} \right\} \tag{5}
$$

The uncertainties due to statistical considerations in the components can be calculated from estimation theory to be

$$\Delta u = \left(z_c/\sqrt{N}\right)s_u$$
$$\Delta v = \left(z_c/\sqrt{N}\right)s_v \tag{6}$$
$$\Delta w = \left(z_c/\sqrt{N}\right)s_w$$

where z_c is the confidence coefficient and N is the number of realizations per channel. For a normal distribution and a confidence level of 95%, z_c has a value of 1.96. Equations (5) and (6) allow calculation of the uncertainty in the u,v and w velocity components from the standard deviation in each of the LDA channels when N is known. Conversely, they can be used on-line in the data aquisition software to calculate the value of N which is required to yield a desired uncertainty level, by obtaining s_1, s_2 and s_3 from a preliminary sample measurement at that point.

In order to estimate the statistical uncertainty in the data presented, two components of Eq.(6) are written

$$\Delta u/u = \left(z_c/\sqrt{N}\right)s_u/u$$
$$\Delta v/v = \left(z_c/\sqrt{N}\right)s_v/v \tag{7}$$

where s_u/u and s_v/v are the turbulence intensities along the x and y coordinate directions. Note that the third velocity component has been omitted from this consideration. Assuming isotropic turbulence, the uncertainty in V can then be approximated by

$$\Delta V/V \le \sqrt{2/N}\left\{s_V/V\right\}z_c \tag{8}$$

with a maximum turbulence intensity of 20% in the 1.6 case and 10% in the 1.3 case and with 1000 realizations per channel the uncertainty in the velocity due to statistical considerations is computed using Eq.(8) to be approximately 2% in the 1.6 case and 1% in the 1.3 case. The resulting uncertainty in the Mach number due to statistical considerations is 3% in the 1.6 case and 1.5% in the 1.3 case.

As noted by Orloff and Snyder (ref. 22), in order to determine the matrix elements in Eq.(4) as accurately as possible, great care must be exercised in calibrating the LDA system when the angle ϕ is small. If this precaution is not observed, large systematic uncertainty can arise in the calculated z velocity component. Systematic uncertainty in the x and y velocity components is considered to be very small, and therefore has not been considered in the uncertainty analysis.

The overriding concern with an LDA system of this type (i.e., one where ϕ is small) is the uncertainty in the w component, since the uncertainty in u and v will be very small given a reasonable N. This particular problem due to LDA system geometry (being a subset of the generalized 3-D LDA system) has been investigated by Neti and Clark (ref. 23) and Yanta (ref. 24). They found the uncertainty in w to be dependent on the turbulence intensity, N, ϕ and the flow angle.

From these studies and preliminary measurements it was determined that to achieve approximately the same resolution in w, as in u and v, 8000 realizations would be required in each of the v_1 and v_3 channels and that measurements should be restricted to areas where the flow angle in the x-z plane is expected to be greater than 3°. The well behaved results tend to support this analysis.

It should also be mentioned that velocity bias was not considered for this investigation, but is expected to be very small due to the high data rates encountered in both flowfields.

The uncertainty in the Mach number from statisical considerations and from ignoring the w component in regions in which it was not measured is therefore approximately 6% and 3% for 1.6 and 1.3 cases respectively.

RESULTS AND DISCUSSION

Flow Visualization Results

For the Mach 1.6 case, schlieren photographs reveal that the shock becomes bifurcated as it approaches the boundary layer. This behavior is shown in Fig. 7 and was also observed in previous two-dimensional experiments. The photograph indicates reflections arising from the rear legs of the lambda shocks which cross near the tunnel centerline. These phenomena have not been observed in the two-dimensional case. It also shows a slip line extending downstream of the bifurcation point which arises from the air flow on either side having passed through different shock systems. The surface oil flow visualization indicates that there are large separation regions in the corners of the tunnel near the interaction region. This is shown in Fig. 8. These separated flow regions contribute to the three-dimensional nature of the interaction and impart a nozzle effect which together with the thickening of the boundary layer in the vicinity of the shock causes the reacceleration in the freestream behind the normal shock. This reacceleration region terminates at the secondary shock whereupon it reaccelerates and shocks down once more before leaving the test section.

For the Mach 1.3 case, the schlieren photographs, shown in Fig. 9, reveal a different shock structure from that found in the Mach 1.6 case. The shock degenerates as it approaches the boundary layer with no indication of a lambda shock, as in the 1.6 case. Figure 9 does indicate weak oblique shocks forward of the main shock which terminate in the boundary layer. This appears to be a precursor of the forward leg of the lambda shock that appears in the higher Mach number flows. Oil flow visualization indicates that no or very isolated corner separation occurs in the Mach 1.3 case. This is shown in Fig. 10.

Surface Static Pressure Measurements

The floor static pressure distributions for the two test cases were normalized to the upstream mid-span static pressure and are plotted in Figs. 11 and 12. These plots show the symmetry of the flow as well as a sweeping forward of the pressure gradient in the corners. This is more pronounced in the 1.6 case, indicating a sweeping forward of the front legs of the lambda as was also confirmed in the LDA results.

LDA Results

The results of the Mach 1.6 investigation show that the flow follows the one-dimensional normal shock relationships only in the center of the tunnel, and then, only immediately downstream of the shock. This flow is reaccelerated to become supersonic and then experiences a much weaker set of secondary shocks. This can be seen in Fig. 13. The growth in the boundary layer due to the adverse pressure gradient is also indicated. Just downstream of the bifurcation point a slip line can

be seen as has been indicated in previous two-dimensional investigations. The slip line is obscured further downstream due to the reacceleration in the freestream and the secondary shocks associated with the three-dimensionality of the flow.

Although LDA surveys were made near the corner, as close as 1 cm (0.4 inches) from the sidewall and floor, no reverse flow was ever detected. The lowest velocity measured in this region was approximately 100 m/s (328 fps). The cross section data for the Mach 1.6 case are plotted in Fig. 14. A sweeping forward of the front legs of the lambda shock near the corner and a sweeping back of the rear legs are evident. Just downstream of the shock, the flow is subsonic in the freestream, but remains supersonic near the corner. This region extends downstream where it interacts with the reacceleration region and the secondary shocks and then becomes indistinguishable. At this point the boundary layer has become very large. At x = 24cm (9.4 inches), the flowfield has just passed through the secondary shock, i.e., the flow in the freestream is slightly slower than that nearer the corner. At x = 30cm (11.8 inches), the flow is about to experience another weak normal shock. At x = 35cm (13.8 inches), the flow is nearly uniform in the freesteam and about to exit the test section.

The secondary flow vectors given in terms of Mach number are shown in Fig. 15 for the Mach 1.6 case. The plots show the flow turning away from the walls and corner with little or no secondary flow outside the lambda shock region. The freestream normal shock was maintained at x = 10 cm for both test cases.

The results of the Mach 1.3 investigation indicate a less dynamic, less complicated and more uniform flowfield. As expected, there is no lambda shock. Instead, weak compression waves are seen to extend from the shock into the boundary layer. Figure 16 indicates that along the tunnel centerline, the flow follows closely the one-dimensional normal shock relations. Downstream of the shock in the freestream, the flow gradually accelerates to just under sonic conditions (Mach 0.99).

There is a region of high-speed flow in the corner just downstream of the shock as in the Mach 1.6 case. This supersonic region remains isolated in the corner and becomes smaller and smaller downstream. This is shown in the series of plots in Fig. 17. At the exit of the test section, this region of supersonic flow nearly vanishes, while the remainder of the flowfield is choked.

The secondary flow plots for the 1.3 case (Fig. 18) indicate very little secondary flow relative to the 1.6 case. The plotted results indicate that the slight flow turning is near the limit of resolution for the LDA system which is a function of the flowfield turbulence and flow angle. The plots indicate a tendency of the flow to turn away from the corner as in the 1.6 case. A vortical flow is indicated in the x = 10 cm plot which is at the shock location.

CONCLUDING REMARKS

The test results reveal that the structure of the shock system, the three-dimensionality and the extent of separation are highly dependent on Mach number. The flowfield associated with the Mach 1.3 interaction is much more uniform and two-dimensional than that found in the Mach 1.6 case. Extensive separation and hence three-dimensionality (in the Mach 1.6 case) caused regions of strong acceleration downstream of the initial shock, thereby inducing a complicated secondary shock system. This causes a consequent erosion of the energy contained in the flow as well

748

as strong non-uniformities across the flow. Since this is generally undesirable, these tests confirm the general rule of inlet design where normal shocks are designed to occur only at Mach numbers of 1.3 and below.

Efforts are currently under way to investigate the periodic nature of the shock motion from the LDA data already obtained in addition to planning future experimental studies into the unsteady nature of the flow.

REFERENCES

1. Seddon, J., "Flow Produced by Interaction of a Turbulent Boundary Layer with a Normal Shock Wave of Strength Sufficient to Cause Separation," Brit. Aero. Res. Council, Rept. and Memo. No. 3502, March 1960.

2. Chapman,D.R.,Kuehn,D.M. and Larson,H.K., "Investigation of Separated Flows in Supersonic and Subsonic Streams with Emphasis on the Effect of Transition," NACA Rept. 1356, 1958.

3. Mateer,G.G.,Brosh,A. and Viegas,J.R., "A Normal Shock Wave Turbulent Boundary Layer Interaction at Transonic Speeds," AIAA Paper No. 76-161, January 1976.

4. Liepmann,H.W., "The Interaction Between Boundary Layers and Shock Waves in Transonic Flow," Journal of Aeronautical Sciences, Vol. 13, No. 12, 1946, pp. 623-637.

5. Ackert,J.,Feldmann,F. and Rott,N., "Investigations of Compression Shocks and Boundary Layers in Gases Moving at High Speed," NACA TM 1113, Washington,D.C., January 1947.

6. Green,J.E., "Interactions Between Shock Waves and Turbulent Boundary Layers," Royal Aircraft Establishment Technical Report 69098, May 1969.

7. Vidal,R.J.,Wittliff,C.E.,Catlin,P.A. and Sheen,B.H., "Reynolds Number Effects on the Shock Wave/Turbulent Boundary Layer Interaction at Transonic Speeds," AIAA Paper No. 73-661, 6th Fluid and Plasma Dynamics Conference, Palm Springs, California, July, 1973.

8. Klemm,W.J., A Prediction of the Interaction of a Normal Shock Wave with a Separating, Turbulent Boundary Layer, PhD Dissertation, Dartmouth College, 1978.

9. LeBlanc,R. and Goethals,R., "Study of Normal Shock Wave/ Turbulent Boundary Layer Interaction Phenomena in View of Application to Transonic Turbomachines," NASA Technical Translation F-16698, Washington, D.C., December 1975.

10. Kooi,J.W., "Experiment on Transonic Shock Wave Boundary Layer Interaction," National Aerospace Laboratory, the Netherlands, 1975.

11. Mateer,G.G. and Viegas,J.R., "Effect of Mach Number and Reynolds Number on a Normal Shock Wave/Turbulent Boundary Layer Interaction," AIAA Paper No. 79-1502, 1979.

12. Delery,J.M., "Experimental Investigation of Turbulence Properties in Transonic Shock/Boundary Layer Interactions," AIAA Journal, February 1983, p. 180.

13. Om,D., Childs, M.E. and Viegas, J.R., "An Experimental Investigation and Numerical Prediction of a Transonic Normal Shock Wave/Turbulent Boundary Layer Interaction," AIAA Paper No. 82-0990, 1982.

14. Abbiss, J.B., East, L., Nash, C., Parker, P., Pike, P., and Sawyer, W.G., "A Study of the Interaction of a Normal Shock Wave and a Turbulent Boundary Layer Using a Laser Anemometer," Royal Aircraft Establishment Technical Report 75141, Dec. 1975.

15. East, L.F., "The Application of a Laser Anemometer to the Investigation of Shock Wave Boundary Layer Interactions," Royal Aircraft Establishment Technical Memorandum Aero. 1666, February, 1976.

16. Liu, B.Y.H., Whitby, K.T. and Yu, H.H.S., "A Condensation Aerosol Generator for Producing Monodispersed Aerosols in the Size Range $0.036\mu m$ to $1.3\mu m$," Journal de Recerches Atmospheriques, 1966.

17. Yanta, W.J., "Measurements of Aerosol Size Distributions with a Laser-Doppler Velocimeter," National Bureau of Standards Special Publication 412, May 1974.

18. Chriss, R.M., Keith, T.G. and Hingst, W.R., "An Evaporation-Condensation Aerosol Generator for LDV Seeding in a Supersonic Wind Tunnel," Particulate and Multiphase Processes, ed. Ariman, T. and Veziroglu, T.N., Vol. 2, p. 347.

19. Maxwell, B.R., Seasholtz, R.G., "Velocity Lag of Solid Particles in Oscillating Gases and in Gases Passing Through Shock Waves," NASA TN D-7490, March 1974.

20. von Stein, H.D. and Pfeifer, H.J., "Investigation of the Velocity Relaxation of Micron Sized Particles in Shock Waves Using Laser Radiation," Applied Optics, Vol. 11, No. 2, February 1972.

21. Snyder, P.K., Orloff, K.L. and Reinath, M.S., "Reduction of Flow Measurement Uncertainties in Laser Velocimeters with Nonorthogonal Channels," AIAA Journal, Vol. 22, August 1984.

22. Orloff, K.L. and Snyder, P.K., "Laser-Doppler Anemometer Measurements Using Nonorthogonal Velocity Components: Error Estimates," Applied Optics, Vol. 21, January 1982.

23. Neti, S. and Clark, W., "On-Axis Velocity Component Measurement with Laser Velocimeters," AIAA Journal, Vol. 17, No. 9, pp. 1013-1015, Sept. 1979.

24. Yanta, W.J., "The Use of the Laser Doppler Velocimeter in Aerodynamic Facilities," AIAA Paper No. 80-0435-CP, March 1980.
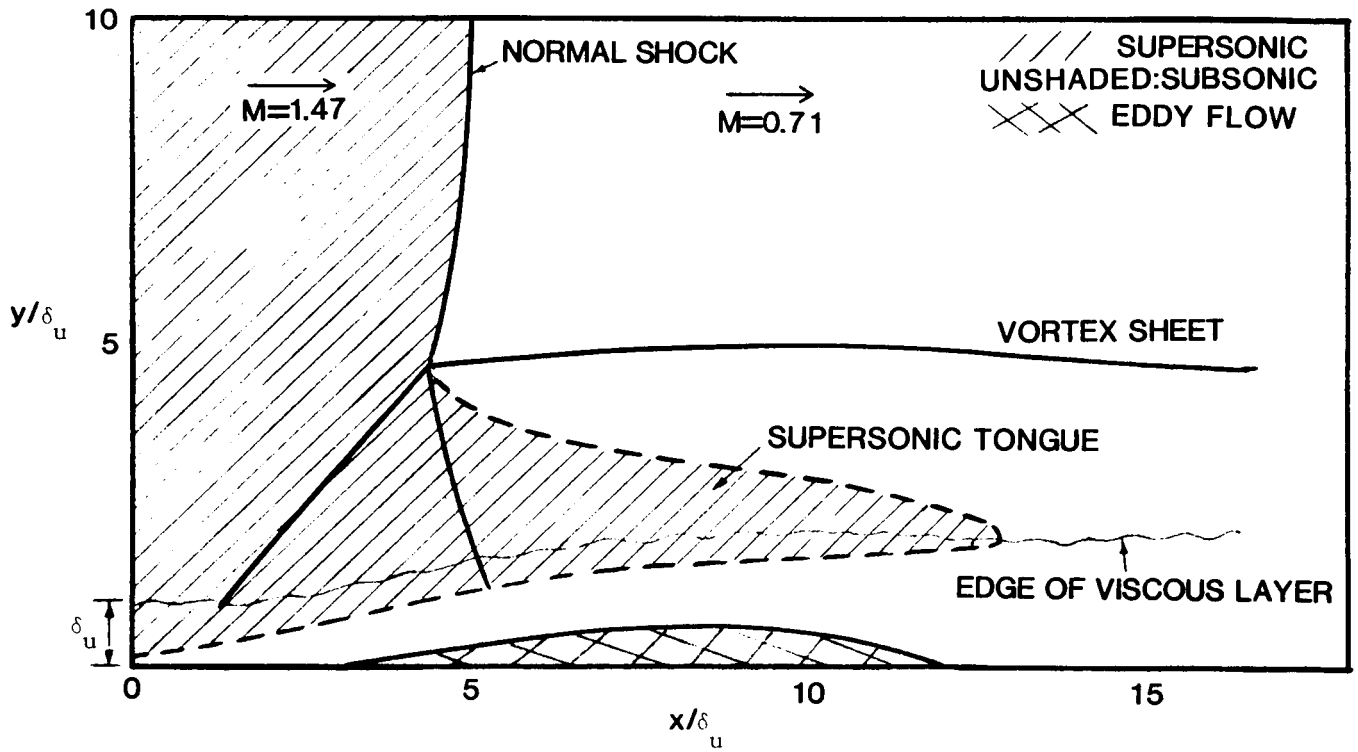
Fig. 1. Seddon's benchmark model of 2-D normal shock wave boundary-layer interaction.
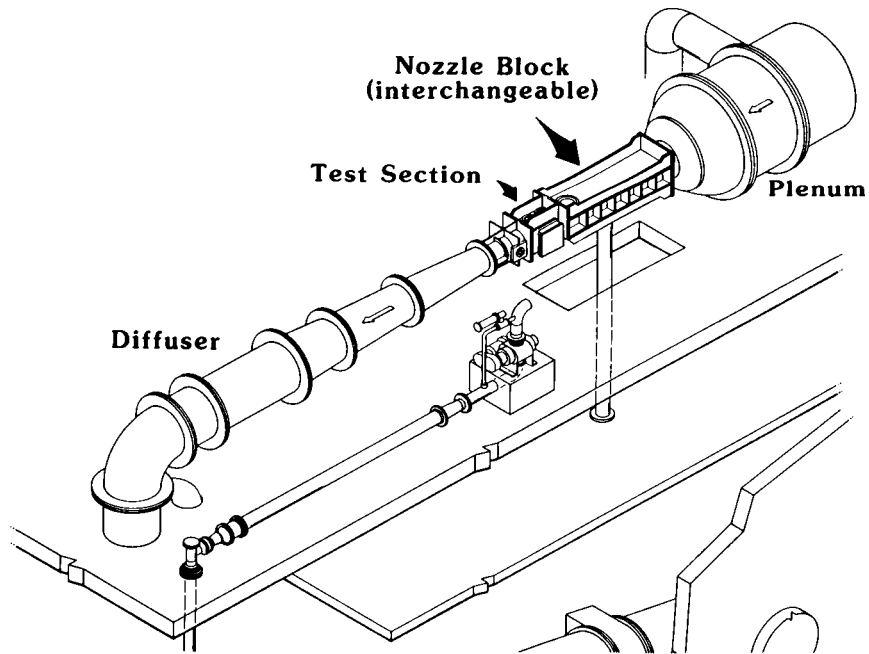
Fig. 2. NASA Lewis Research Center's 1 ft x 1 ft supersonic wind tunnel.
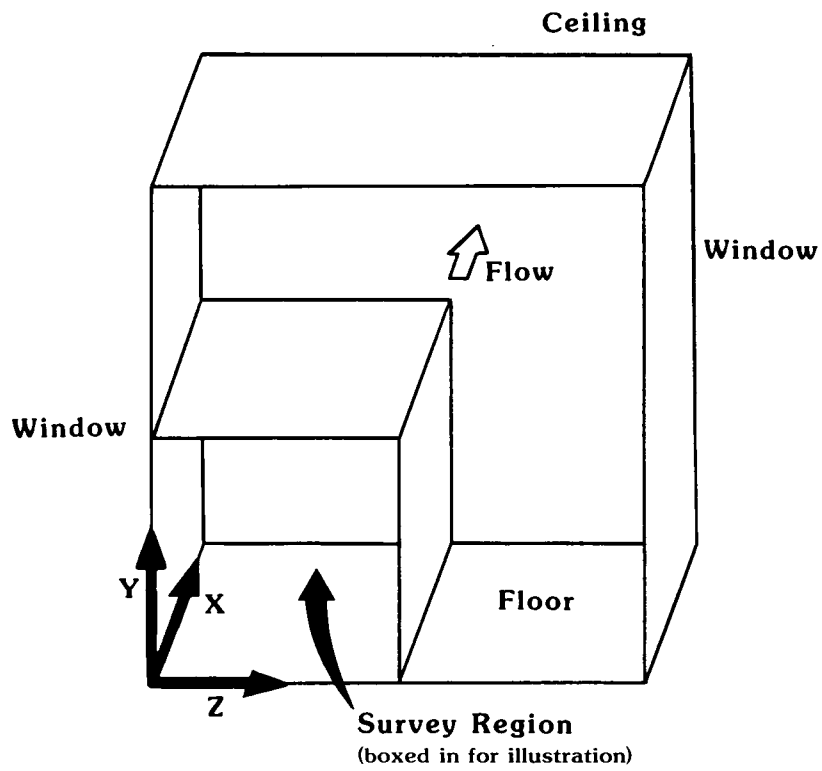
Fig. 3. Test section coordinate system.
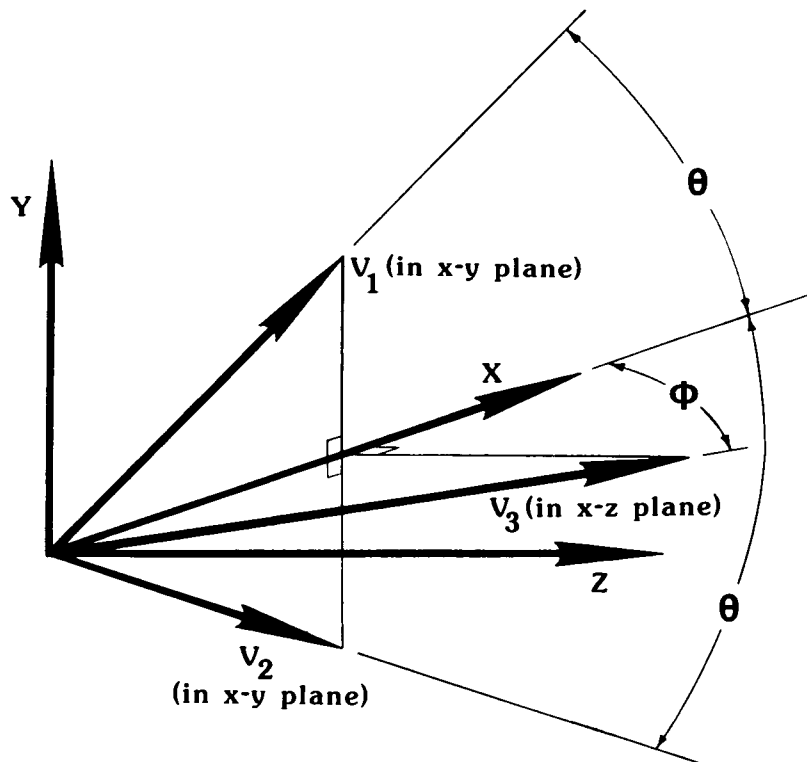
Fig. 4. Nonorthogonal LDA channels.
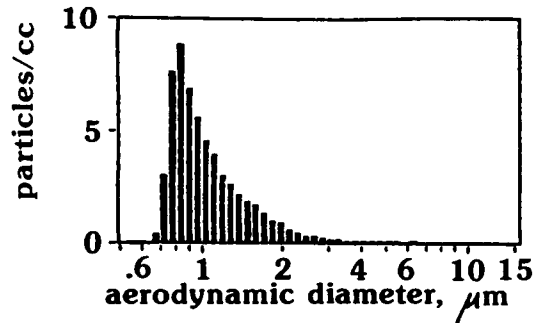
(a) Tunnel Ambient (no seed)
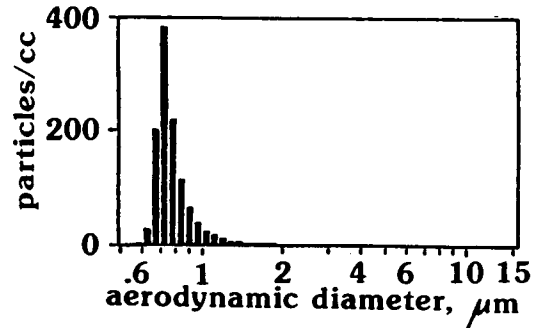
(b) With Seed Added

Fig. 5. Comparison of air samples taken from tunnel test section at test conditions with TSI, Inc. APS 33.
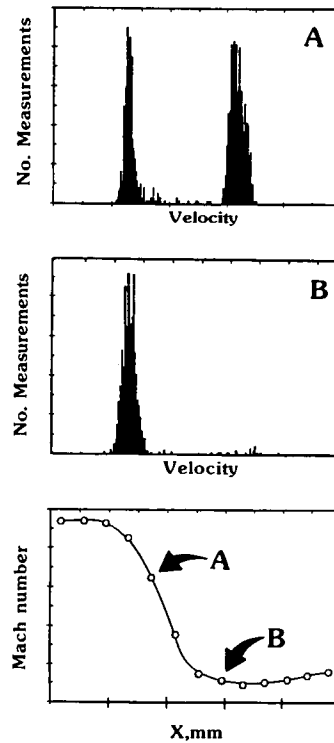
Fig. 6. Sample histograms taken as shock wave oscillates about the LDA probe volume.
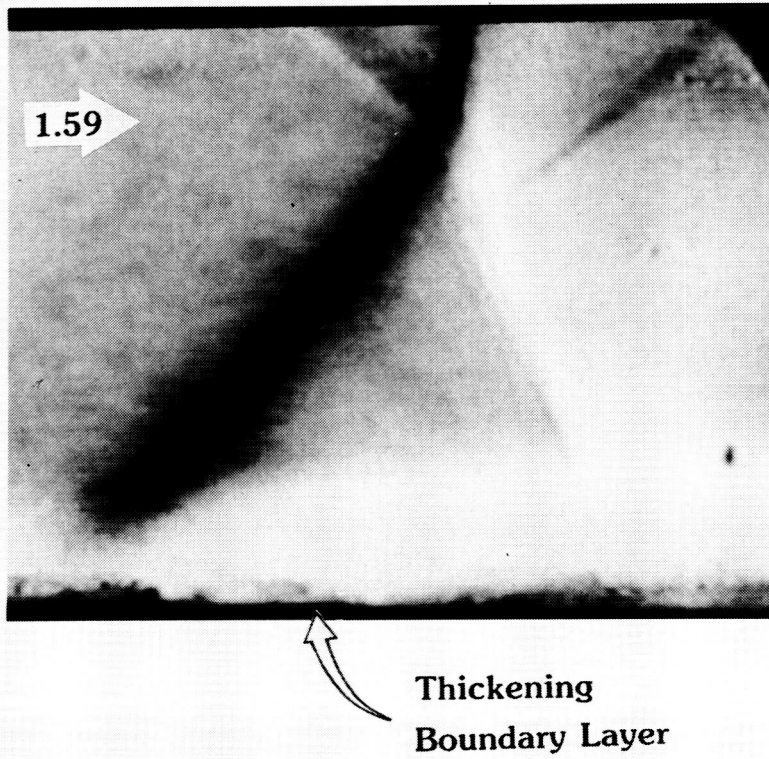
Fig. 7. Schlieren photograph taken at Mach 1.59.
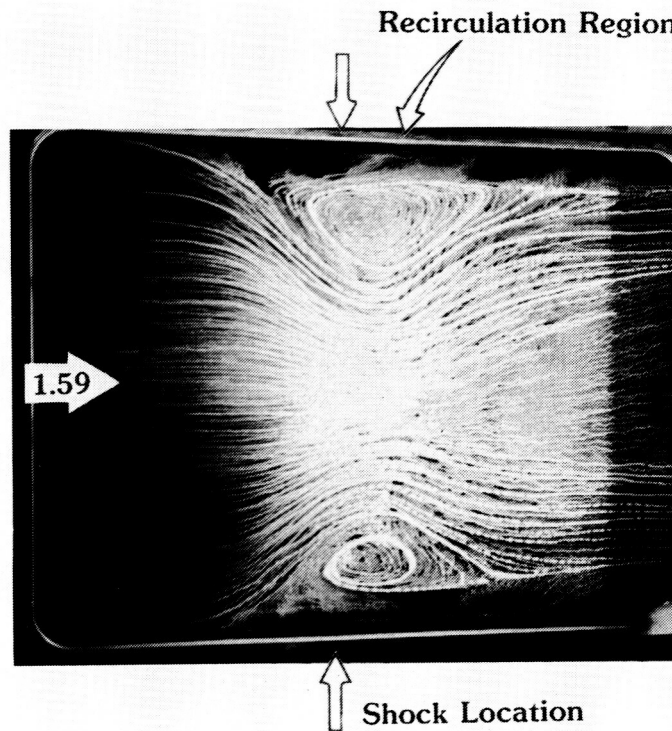
Fig. 8. Surface oil-flow pattern at Mach 1.59.
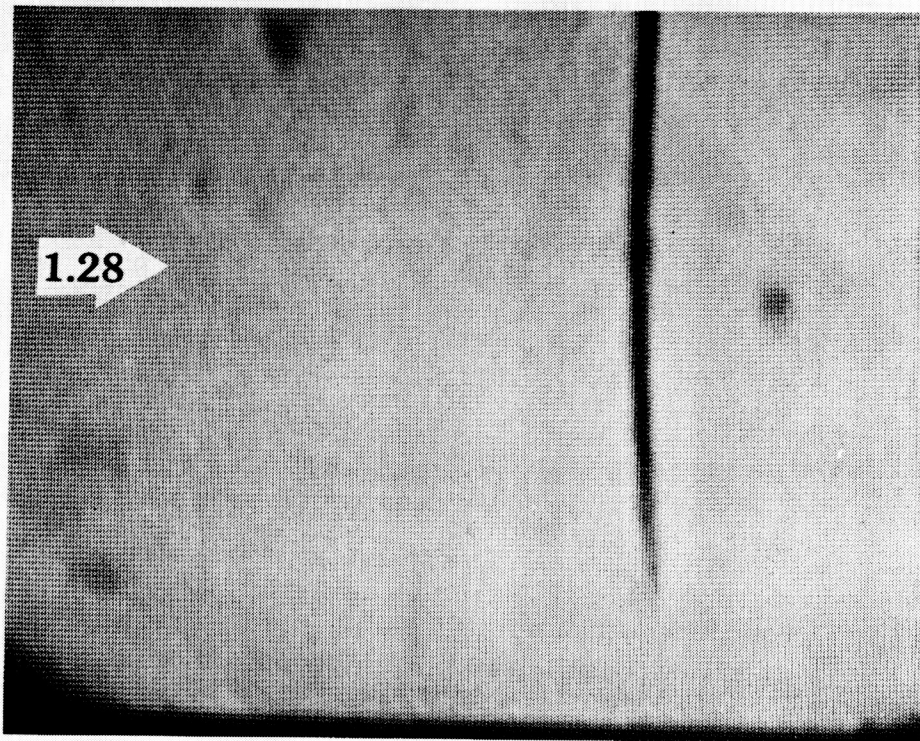
Fig. 9. Schlieren photograph taken at Mach 1.28.
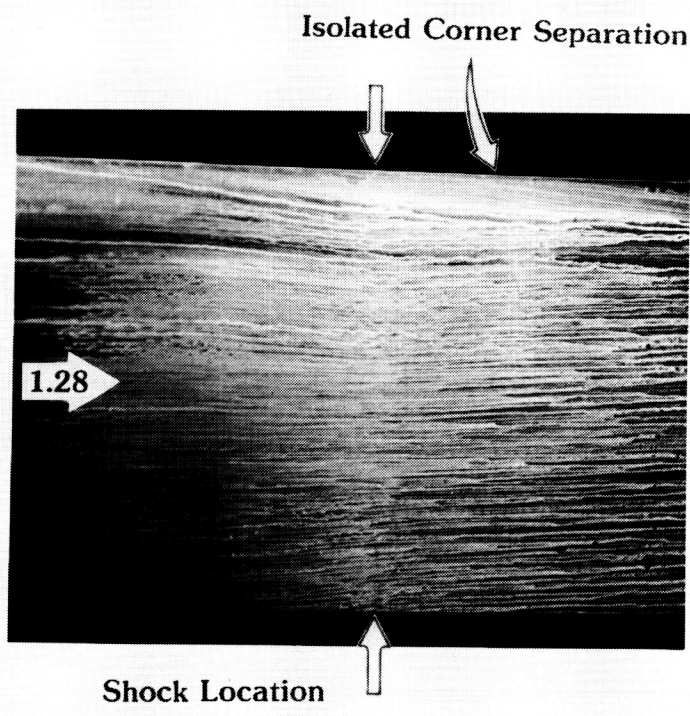
Fig. 10. Surface oil-flow pattern at Mach 1.28.
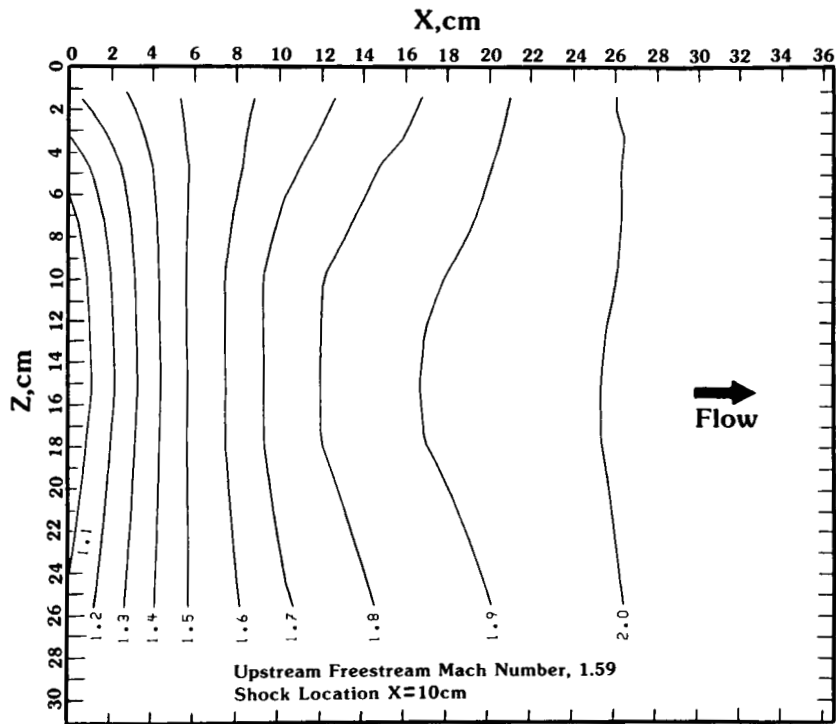
Fig. 11. Floor surface static pressure contours of the Mach 1.6 flow field, normalized to mid-span upstream static.
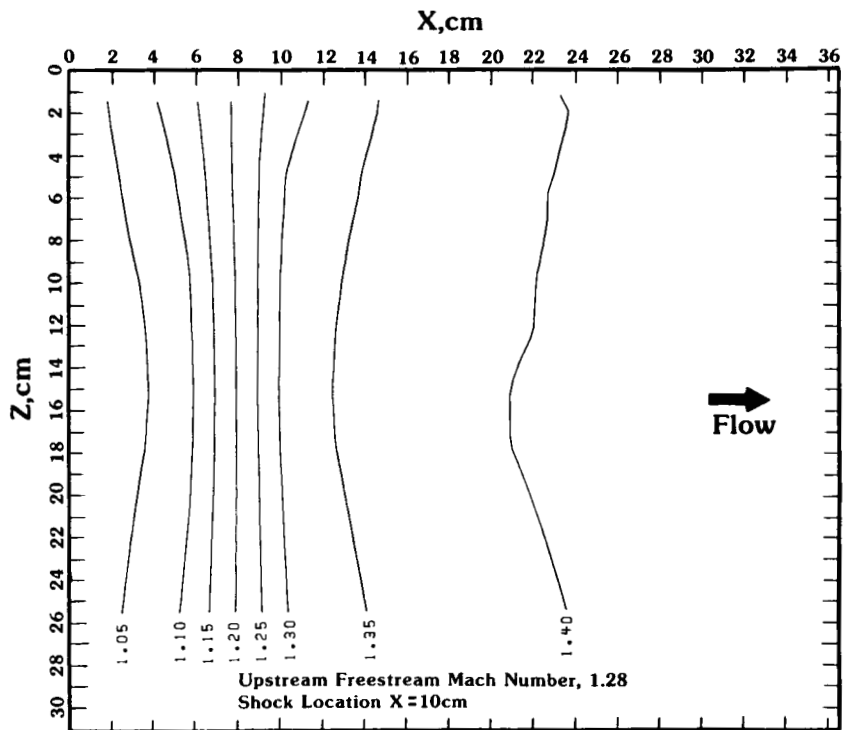
Fig. 12. Floor surface static pressure contours of the Mach 1.3 flow field, normalized to mid-span upstream static.

756
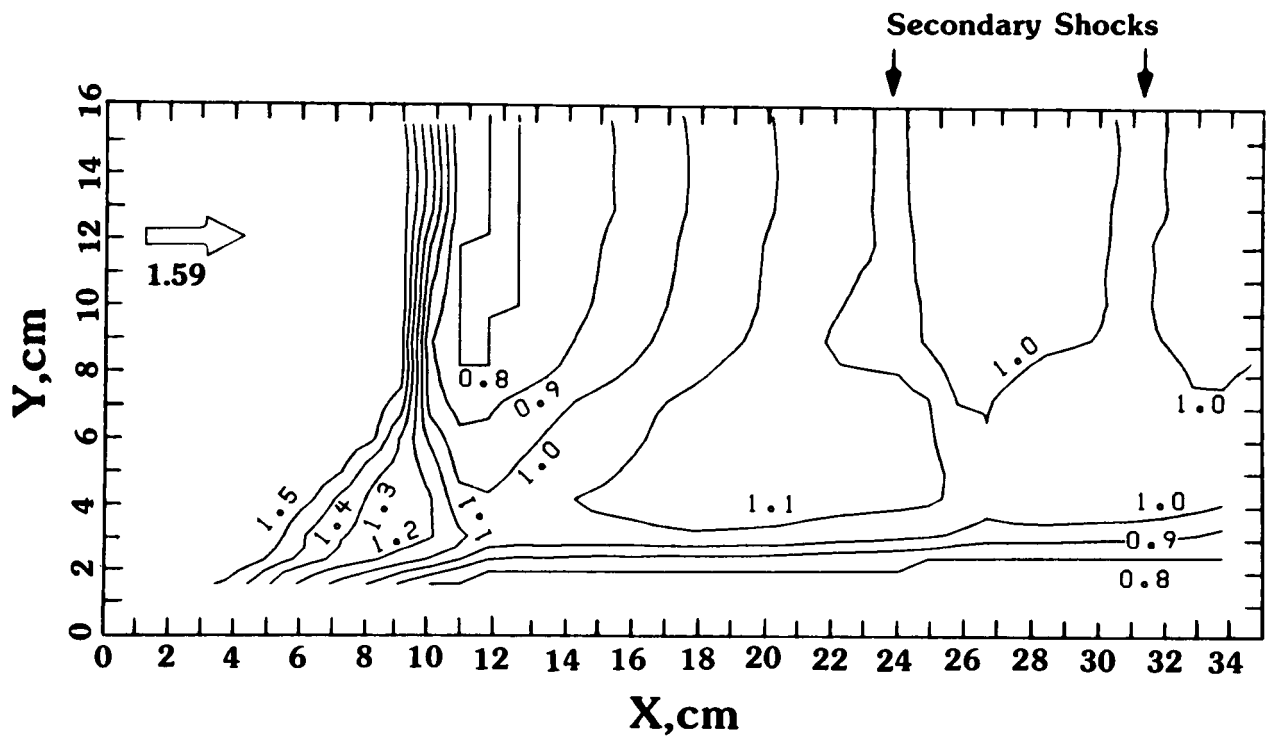
Fig. 13. LDA mid-span Mach number contours (z = 15cm) for the Mach 1.6 test case.
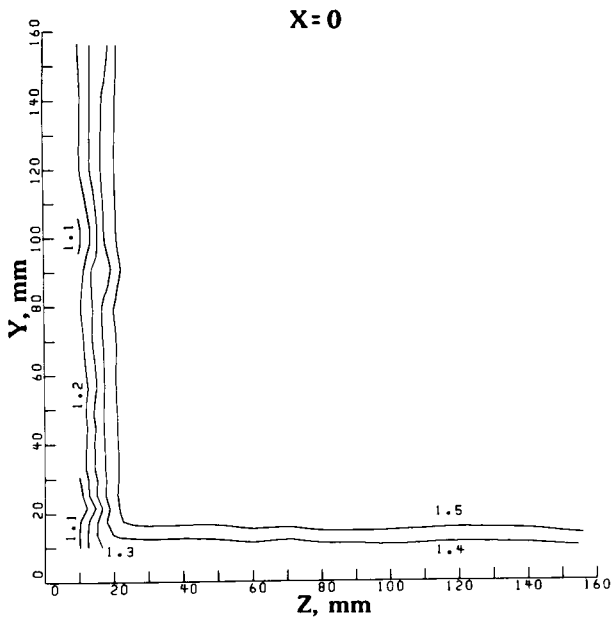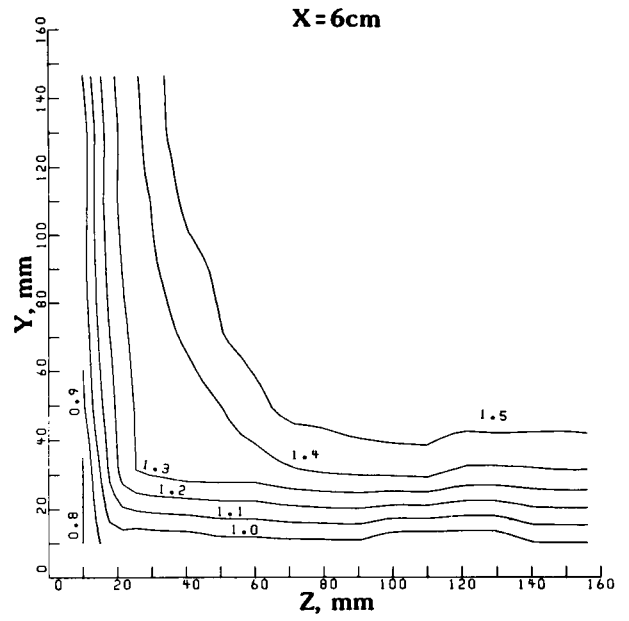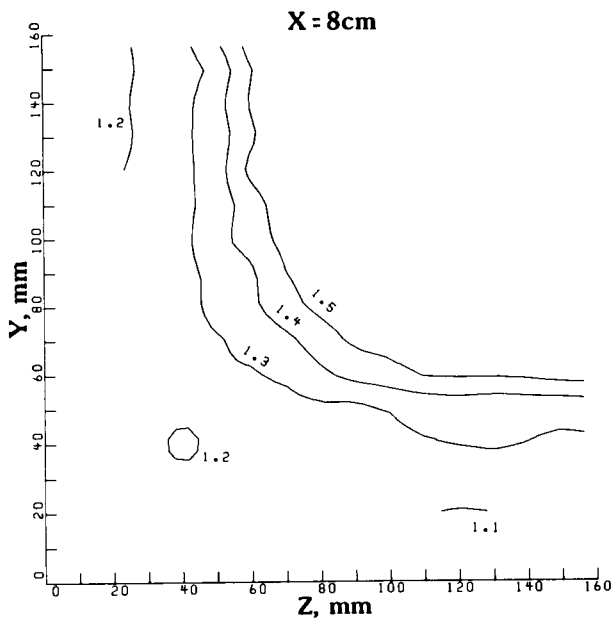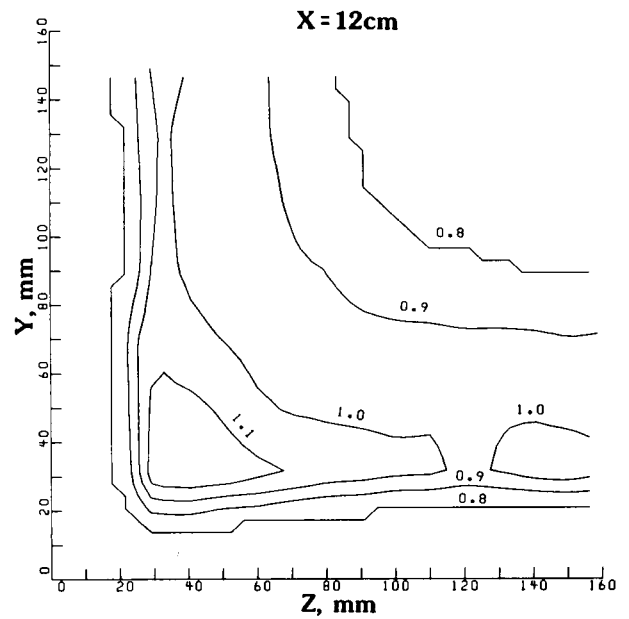
Figure 14. LDA cross-section Mach number contours for Mach 1.6 test case.
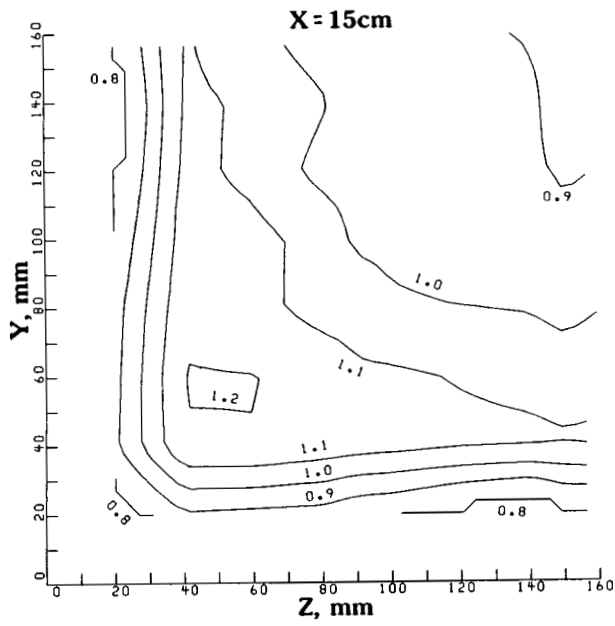
(e)
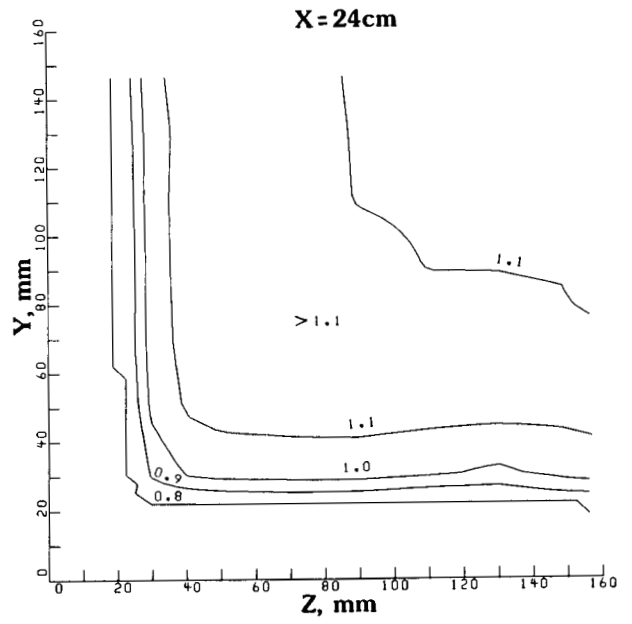
(f)
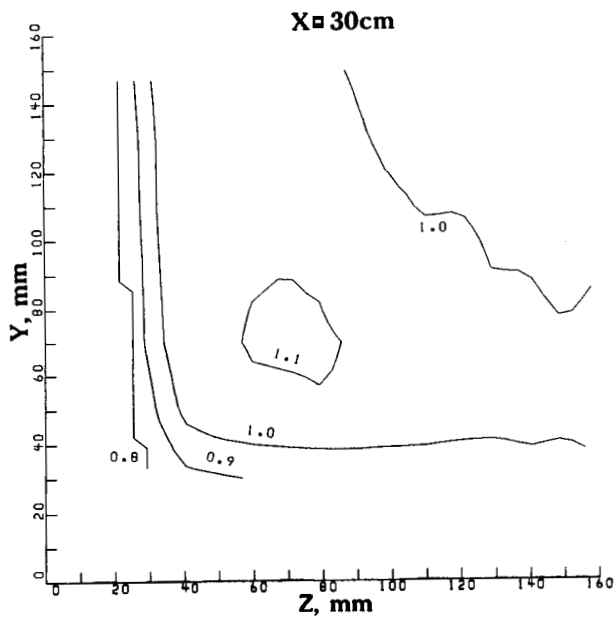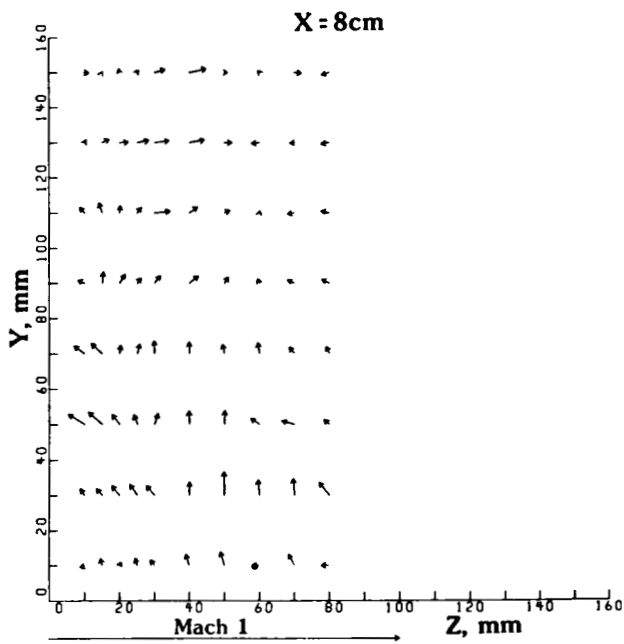
(g)
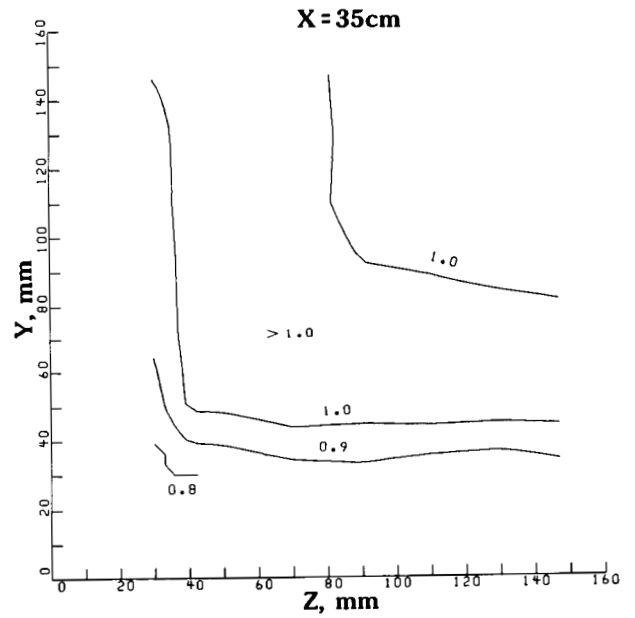
(h)

Figure 14. Concluded.

759
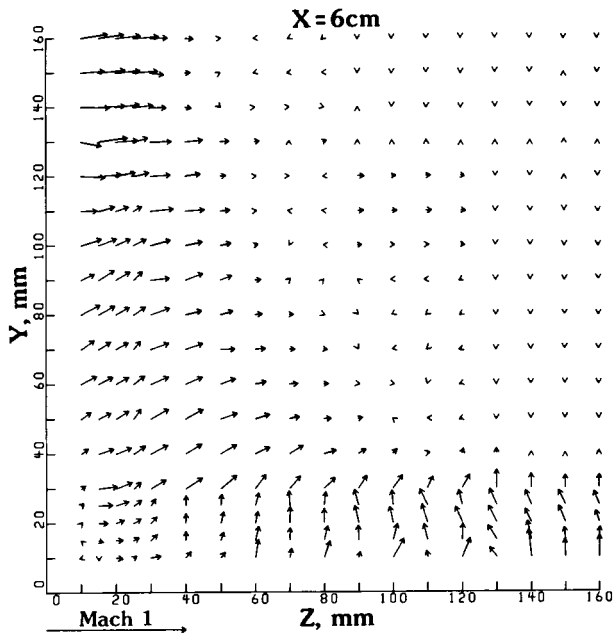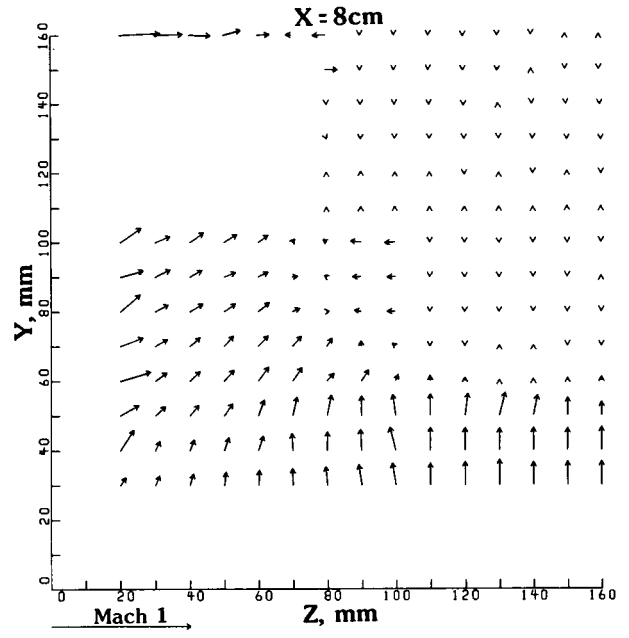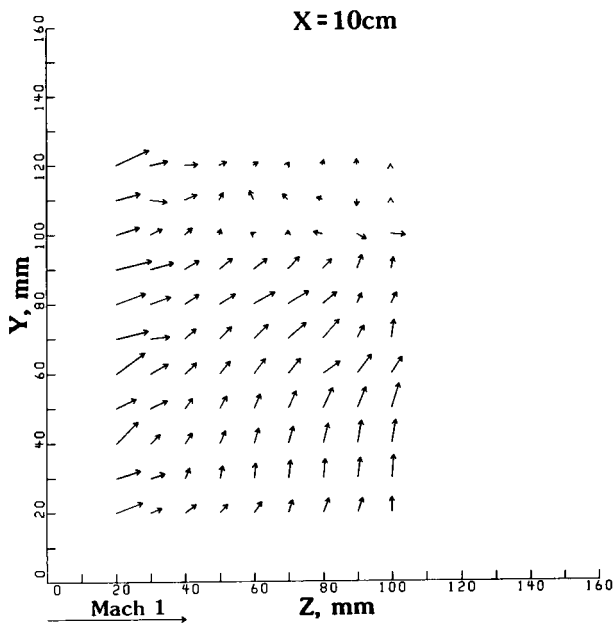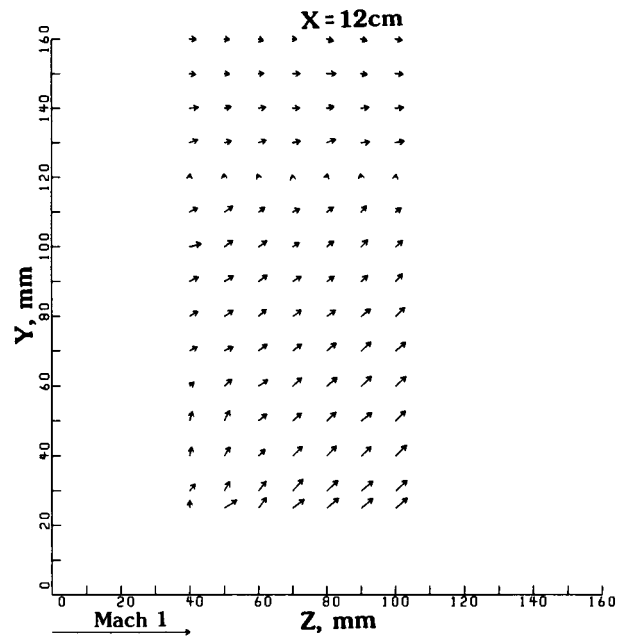
Figure 15. Secondary flow vectors for Mach 1.6 test case.
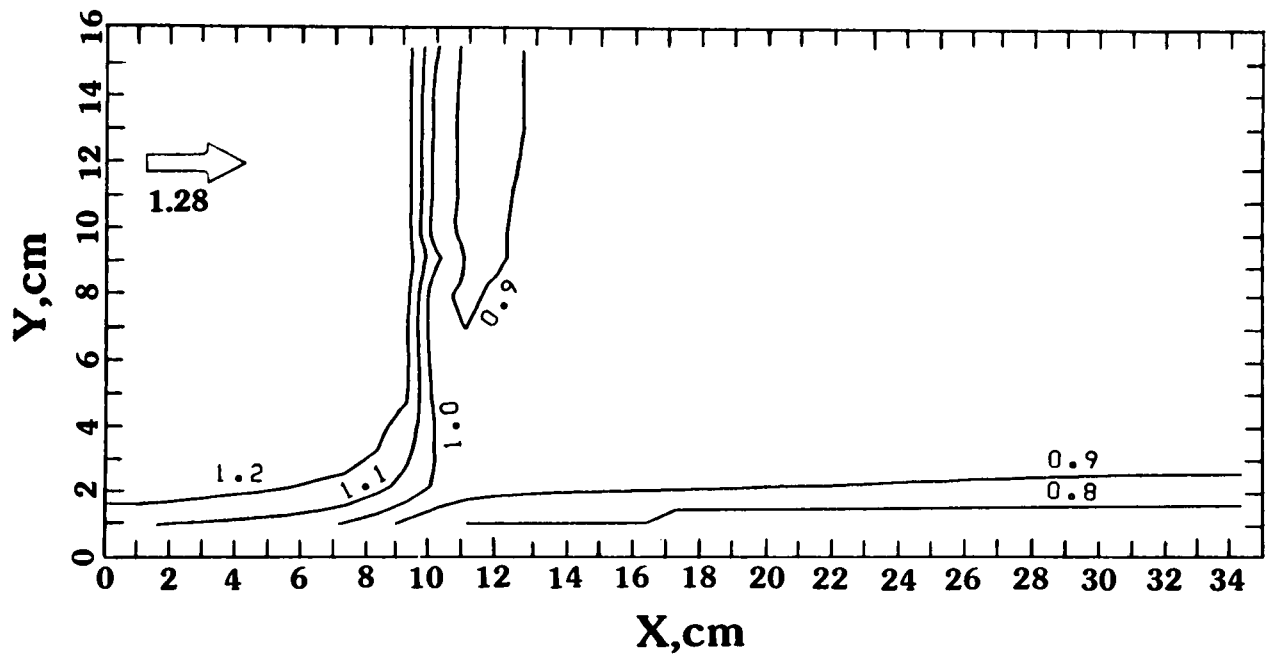
Fig. 16. LDA mid-span Mach number contours (z = 15cm) for the Mach 1.3 test case.
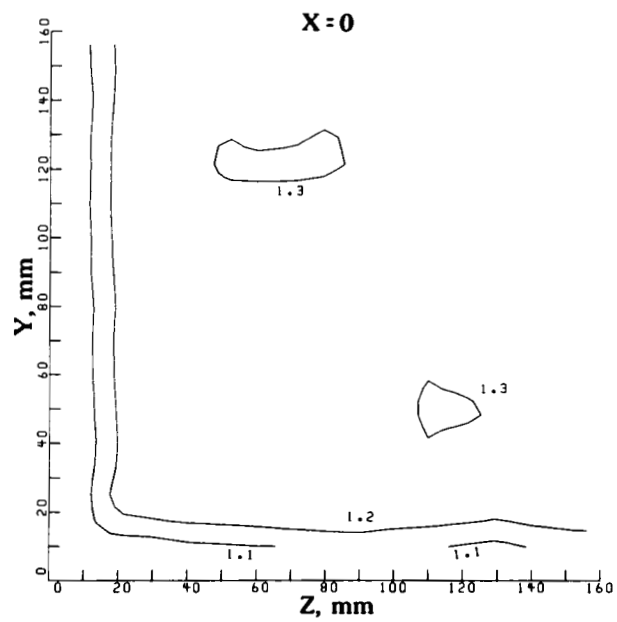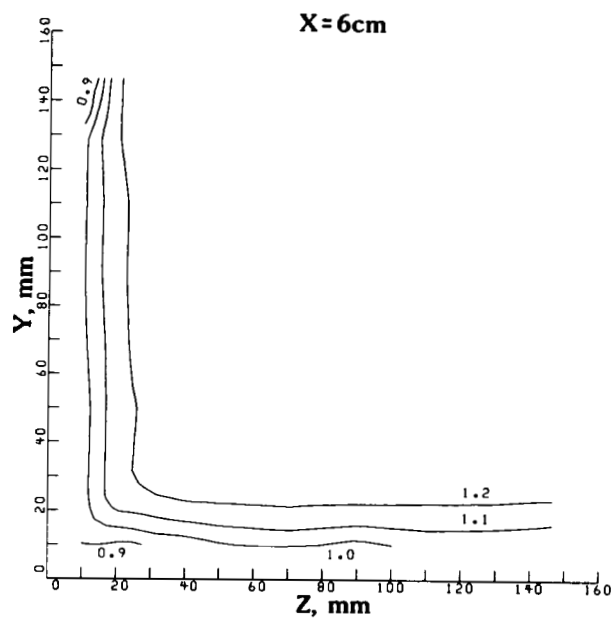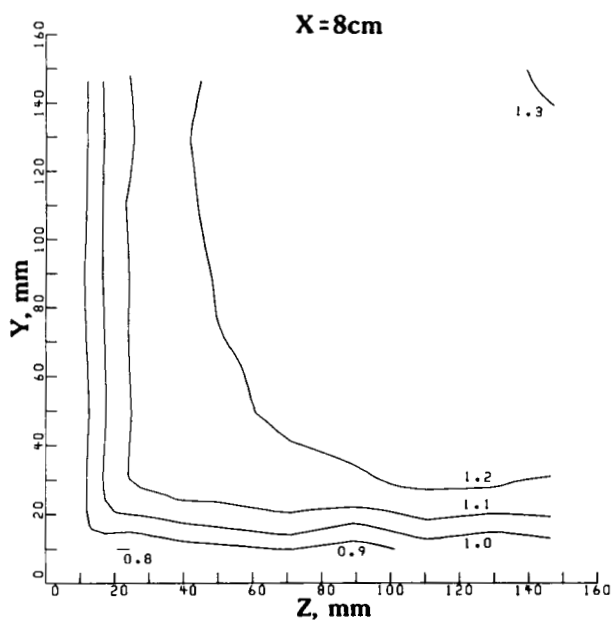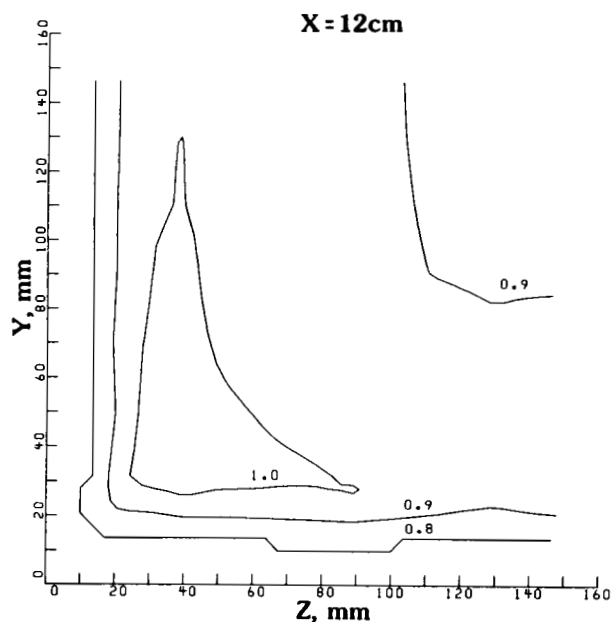
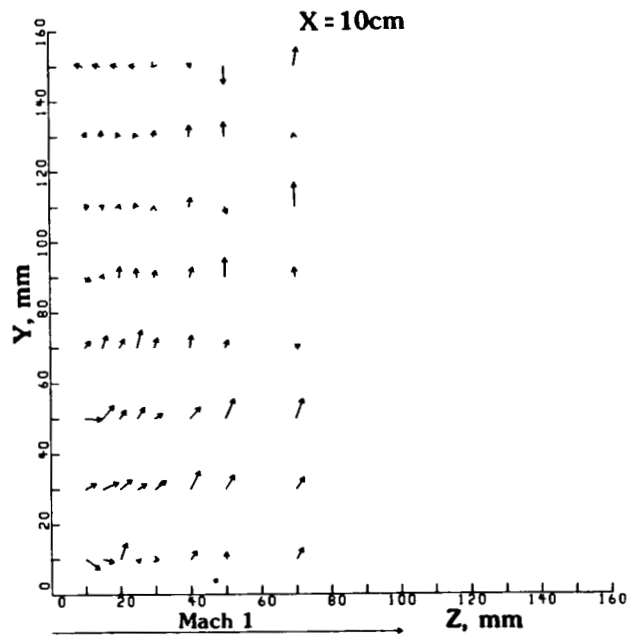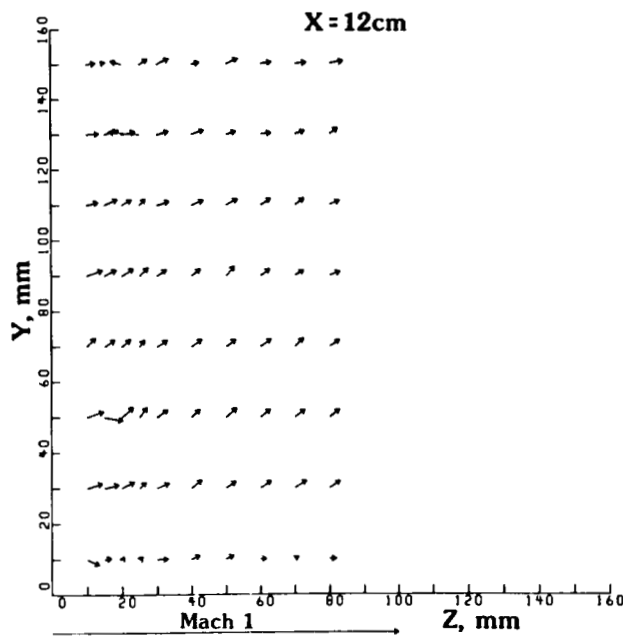Figure 17. LDA cross-section Mach number contours for Mach 1.3 test case.
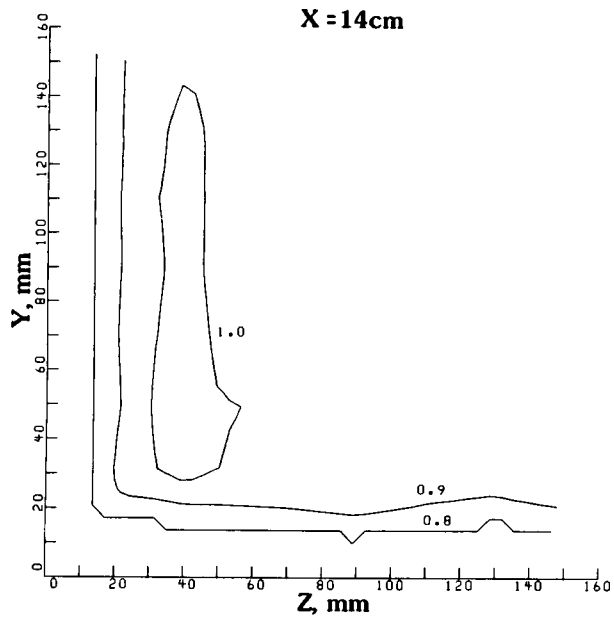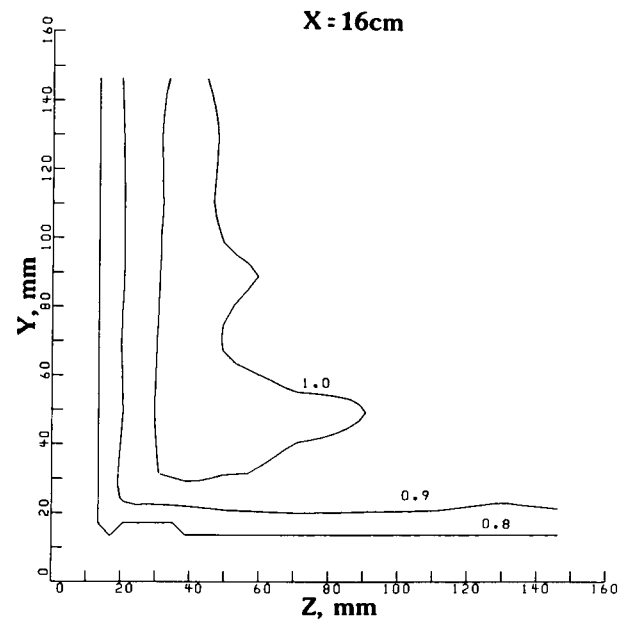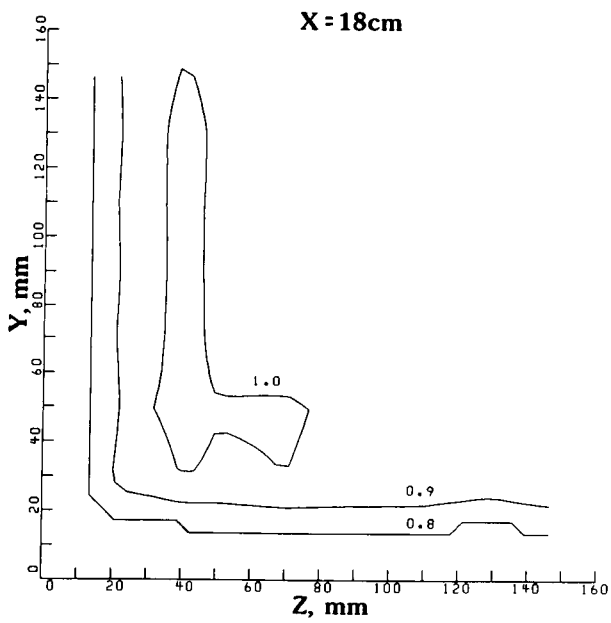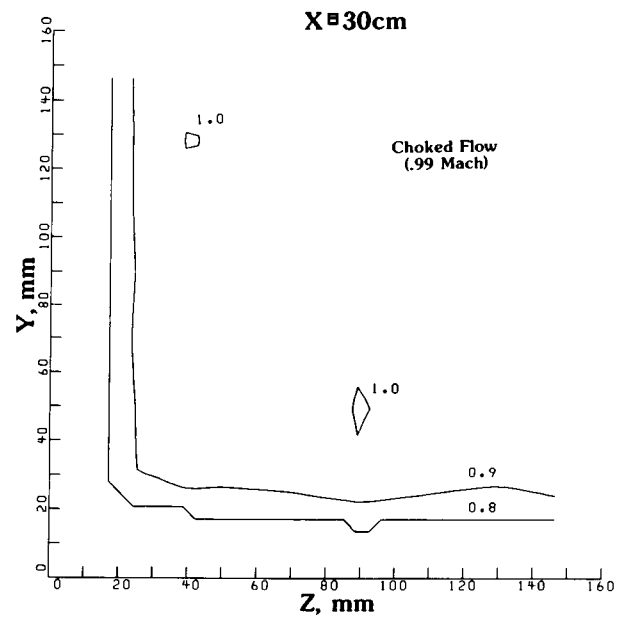
Figure 17. Concluded.

Figure 18. Secondary flow vectors for Mach 1.3 test case.